LAWRENCE
LIVERMORE
NATIONAL
LABORATORY

LLNL-JRNL-648129

L-shell dielectronic satellite transitions of Fe XVII

P. Beiersdorfer, M. P. Bode, Y. Ishikawa, F. Diaz

January 3, 2014

Astrophysical Journal

Disclaimer

This document was prepared as an account of work sponsored by an agency of the United States government. Neither the United States government nor Lawrence Livermore National Security, LLC, nor any of their employees makes any warranty, expressed or implied, or assumes any legal liability or responsibility for the accuracy, completeness, or usefulness of any information, apparatus, product, or process disclosed, or represents that its use would not infringe privately owned rights. Reference herein to any specific commercial product, process, or service by trade name, trademark, manufacturer, or otherwise does not necessarily constitute or imply its endorsement, recommendation, or favoring by the United States government or Lawrence Livermore National Security, LLC. The views and opinions of authors expressed herein do not necessarily state or reflect those of the United States government or Lawrence Livermore National Security, LLC, and shall not be used for advertising or product endorsement purposes.

L-shell dielectronic satellite transitions of Fe XVII

P. Beiersdorfer[1,2], M. P. Bode[2], Y. Ishikawa[3], and F. Diaz[3]

[1] *Physics Division, Lawrence Livermore National Laboratory, Livermore, CA 94550, USA*

[2] *Space Sciences Laboratory, University of California, Berkeley, CA 94720, USA*

[3] *Department of Chemistry and the Chemical Physics Program, University of Puerto Rico, San Juan, PR 00931, USA*

ABSTRACT

We have used the relativistic multi-reference Møller-Plesset perturbation theory to calculate the positions of the dielectronic satellite transitions involving doubly excited $3\ell 3\ell'$ configurations that are associated with the X-ray spectrum of Fe XVII. A comparison of these positions with the wavelengths employed in astrophysical modeling codes shows discrepancies of up to 36 mÅ. Inspection of the spectrum of Capella recorded with the high energy transmission grating on the *Chandra X-ray Observatory* reveals several features enhanced by Fe XVI lines formed by dielectronic recombination, one of which may be of future diagnostic use as it is fairly well isolated and in large part formed by dielectronic recombination.

Subject headings: atomic processes—line: formation— stars: coronae—stars: individual (Capella)—Sun: X-rays—X-rays: general

1. Introduction

Since their identification in laboratory and solar spectra (Gabriel & Jordan 1969; Gabriel & Paget 1972), dielectronic satellite transitions have played a major role in the analysis of K-shell emission spectra. This has been specially true for dielectronic satellite transitions associated with the emission of the closed-shell heliumlike ions of elements with atomic number $Z \geq 18$, which have been observed in laboratory measurements, the Sun, and in astrophysical sources (Gabriel 1972; Bitter et al. 1979, 2003; Gu et al. 2012); in addition, lower-Z ions also display dielectronic satellite lines (Faucher et al. 1983; Wargelin et al. 2001). The reason for their importance is that they can be used as an accurate diagnostic of electron temperature (Dubau & Volonté 1980).

Dielectronic satellite lines also play a role in L-shell emission spectra. Dielectronic satellite lines to the well known characteristic Fe XVII L-shell lines are produced by electron capture and subsequent radiative decay:

$$1s^2 2s^2 2p^6 + e^- \rightarrow 1s^2 2s^2 2p^5 n\ell n'\ell' \rightarrow 1s^2 2s^2 2p^6 n'\ell' + h\nu \tag{1}$$

or

$$1s^2 2s^2 2p^6 + e^- \rightarrow 1s^2 2s 2p^6 n\ell n'\ell' \rightarrow 1s^2 2s^2 2p^6 n'\ell' + h\nu' \tag{2}$$

The strongest such satellite lines are those with $n, n' = 3$ and $\ell = d$.

Dielectronic recombination is a resonant process, because the energy of the free electron e^- must be such that upon capture into a level $n'\ell'$ it gives off the correct energy to promote a bound electron from an $n = 2$ level to a level $n\ell$. The L-shell dielectronic lines are, however, much weaker than the K-shell dielectronic satellite lines observed in the corresponding heliumlike ion of the same element (P. Beiersdorfer, Ph.D. thesis, Princeton University 1988). Despite their overall weakness, L-shell dielectronic satellite lines can play a role in the spectra of stellar coronae, as discussed for the case of Fe XVIII (Clementson & Beiersdorfer 2013). Moreover, Fe XVI lines with a so-called spectator electron $n'\ell'$ and $n' = 4$ have been observed in the spectrum of Capella observed with the *Chandra* X-ray Observatory. They were used to infer a formation electron temperature of $\log(T) = 6.67 \pm 0.026$ K (Beiersdorfer et al. 2011). Fe XVI lines with $n, n' = 3$ (but not yet with higher principal quantum numbers) formed by dielectronic recombination are included in the AtomDB spetral data base commonly used for the analysis of astropysical spectra (Foster et al. 2013).

Unfortunately, no experimental values for the spectral wavelengths and intensities of the $n' = 3$ dielectronic satellites have yet been produced. As a result, the dielectronic satellites incorporated into spectral models must rely on calculations. AtomDB, for example, relies on dielectronic satellite data calculated by Nilsen (1989). Some of the calculated positions of Fe XVI L-shell lines formed by electron-impact excitation and situated in the 15–18 Å range were shown to be highly inaccurate (Graf et al. 2009). Even modern atomic physics codes, such as the Flexible Atomic Code (FAC) (Gu 2008), which has become a standard spectral analysis package for astrophysical spectra, produce Fe XVI lines that were shown to be accurate only to ±40 mÅ (Graf et al. 2009). This is considerably worse than the spectrsocopic accuracy achieved with the high energy grating spectrometer on *Chandra*. An exception to this general trend have been the results obtained with atomic physics codes based on the relativistic multi-reference Møller-Plesset (MRMP) perturbation theory (Ishikawa et al. 1991; Ishikawa & Vilkas 2001). The transition energies calculated with this method for the collisionally excited L-shell transitions of Fe XVI where found to agree with measurements within the experimental uncertainties (Beiersdorfer et al. 2012; Díaz et al. 2013).

In the following we present the wavelengths of the $n' = 3$ dielectronic satellite lines generated by the MRMP method. Comparing these wavelengths to those calculated by Nilsen (1989) we find differences of up to 36 mÅ. Based on our earlier analysis of the collisionally excited Fe XVI lines (Beiersdorfer et al. 2012), we assume that our calculated wavelengths are accurate to within about 2–4 mÅ. Thus, the new $n = 3$ wavelengths are about an order of magnitude more reliabe than the data employed in current models. Using the new wavelength assignments together with dielectronic resonance strengths calculated with FAC we have searched for possible features related to $n = 3$ dielectronic satellite lines in the spectrum of Capella observed with the HETG spectrometer. Unfortunately, most lines blend with other features, and we have been able to identify only one reasonably isolated $n = 3$ satellite line. We also point out several spectral locations where such lines appear to contribute to excess flux not yet fully modeled.

2. Computational results

An in-depth derivation of the theory and procedures used in the MRMP calculations was given by Ishikawa et al. (1991) and Ishikawa & Vilkas (2001). The code was used recently by Díaz et al. (2013) to produce a complete set of energy levels of singly and doubly excited energy levels of Fe XVI. Here we use these energy levels to derive the wavelengths associated with the $n = 3$ dielectronic satellite lines.

In order to pick out the strongest, and the diagnostically most relevant $n, n' = 3$ dielectronic satellite transitions, we have performed calculations with FAC. The *relative* intensities of lines formed by dielectronic recombination is essentially independent of electron temperature, as the excitation and autoionization energies are to first approximation the same for all $n = 3$ resonances. The relative intensities are in this approximation only a function of the satellite line factor F_2 (Dubau & Volonté 1980):

$$F_2 = \frac{g_s}{g_i} \quad \frac{A_a^{si} A_r^{sf}}{\Sigma_j A_a^{sj} + \Sigma_{f'} A_r^{sf'}} \quad , \tag{3}$$

Here, A_a^{si} is the autoionization rate for decay of upper level $|s\rangle$ to the ground state $|i\rangle$ of the recombing ion; A_r^{sf} is the rate of radiative decay of upper level $|s\rangle$ to lower level $|f\rangle$; g_s and g_i are the statistical weights of the autoionizing level and of the ground state of the target ion, respectively. The sum over f' extends over all levels lower than $|s\rangle$; the sum over $|j\rangle$ extends over all levels which are populated by autoionization of level $|s\rangle$. Our calculations, therfore, included the necessary energy levels, radiative rates, and autoionization rates to produce all Fe XVI lines contibuting to its L-shell spectrum emanating from doubly excited $n = 3$ levels.

The dielectronic resonance strengths produced by the FAC calculations are shown in Fig. 1, where we compare them to those found in the AtomDB data base. The satellite strengths agree rather well, mostly within 10%, although a few much larger deviations can also be found. Typically, such deviations are due to differences in the calculated autoionization rates, or they are due to approximations made in the summation when computing the satellite line factor F_2. The predicted positions vary on the order of tens of mÅ, as discussed in the Introduction. For subsequent calculations, we replaced the wavelengths produced by the FAC calculations with those produced with the MRMP code. In Table 1 we compare the wavelengths derived from the MRMP calculations with those used in AtomDB for those Fe XVI lines that receive the strongest contributions from dielectronic recombination.

Dielectronic recombination is not the only mechanism that contributes to the excitation of the L-shell lines of Fe XVI. Many of the Fe XVI lines are also excited by electron-impact excitation. In fact, all Fe XVI lines measured by Graf et al. (2009) were produced by electron-impact excitation. In order to predict how much emission from a given Fe XVI line is due to electron-impact excitation and how much is due to dielectronic recombination, we have used FAC to also calculate the collisional excitation rates.

Representative results of our collisonal-radiative calculations are shown in Figs. 2 and 3. Unfortunately, the relative contributions from collisional excitation and dielectronic recombination depend on the electron temperature and the relative abundance of neonlike and sodiumlike iron ions. The results shown in Figs. 2 and 3 were produced by assuming equal amounts of neonlike and sodiumlike iron ions; the temperature is assumed to be 600 eV and the electron density is set to 10^{12} cm^{-1}, in accordance with the analysis of the Capella spectrum performed by Behar et al. (2001). We point out that the relative dielectronic satellite contribution increases, if we assume a lower electron temperature, a higher neonlike iron fraction, or a lower sodiumlike iron fraction.

Figures 2 and 3 show that the strongest lines are formed by electron-impact excitation. The contribution from electron-impact excitation is shown in black and red. The black intensity corresponds to the emission of a given line, if the excited upper level were to decay only by photon emission. However, all excited $1s^2 2\ell^7 3\ell' 3\ell''$ upper levels can also decay by autoionization. This process is radiationless and diminishes the intensity of the line emission. Taking autoionization into account results in the line intensities shown in red in Figures 2 and 3. Autoionization is very effective in wiping out the photon emission of the the $3s \rightarrow 2p$ transitions that are located in the spectral range above 16 Å, as shown in Fig. 3. It is less effective in reducing the photon emission of the the $3d \rightarrow 2p$ transitions located in the spectral range near 15 Å and shown in Fig. 2. Most of the strong, collisionally excited lines have recently been identified in the spectrum of Capella, as discussed by Beiersdorfer et al.

(2012).

Figures 2 and 3 show that the dielectronic recombination process overall contributes a rather small amount of emission to the Fe XVI L-shell spectrum. In these figures, the contribution from dielectronic recombination is shown in green, which adds to the emission from collisional excitation shown in red. The dielectronic recombination mechanism leads to only a small enhancement of the strong collisionally excited lines. It contributes almost nothing to the emission of the Fe XVI lines in the 16–18 Å region, as illustrated in Fig. 3. In the 15–16 Å region, there are, however, a few lines that are essentially not formed by electron-impact excitation but are formed only by dielectronic recombination. These are the lines that are typically thought of as dielectronic recombination satellite lines and that are of greatest diagnostic interest. The predicted wavelength of these lines can be found in Table 1.

3. Identification of $n = 3$ dielectronic satellite lines in the spectra of Capella

The identification of Fe XVI L-shell lines in astrophysical spectra has been difficult because these lines are rather weak. Their X-ray energies are around 700–800 eV, which is three times the energy needed to ionize the sodiumlike iron ion. Such high electron energies do not favor a high abundance of sodiumlike iron ions. In addition, the lines are weak because autoionization reduces the photon yield, as we have illustrated in the previous section.

The Fe XVI L-shell lines formed by dielectronic recombination can be expected to be even weaker than those lines formed mainly by electron-impact collisions. Beiersdorfer et al. (2011) identified excess flux on the long-wavelength side of the dominant Fe XVII line commonly referred to as $3C$ at 15.01 Å, which they atributed to a feature formed by dielectronic recombination involving an excited electron in the $n = 4$ shell. Unlike dielectronic satellite lines involving an $n = 4$ electron, those involving only $n = 3$ electrons are not clusted in a single peak, but are distributed over a wide range of wavelengths, as illustrated in Figs. 2 and 3, and we do not benefit from blending among the $n = 3$ satellite lines that could substantially enhance these features.

In Fig. 4 we show a spectrum of Capella in the 14.9–15.5 Å wavelength region. The spectrum was produced by co-adding 298 ksec of observations collected with *Chandra's* high energy transmission grating in plus and minus order. The spectrum is dominated by the strong Fe XVII line $3C$. The second strongest feature is that of line $3D$ at 15.26 Å (Behar et al. 2001).

The Capella spectrum has been fitted (black trace in Fig. 4) using data from ATOMDB,

which were modified for emissivities and wavelengths, as described by Gu et al. (2006); Gu (2009). This fit is shown in the figure. ATOMDB does not include collisional Fe XVI transitions; however, as we have mentioned earlier, it includes the $n = 3$ dielectronic satellites. For our analysis, the $n = 3$ flux was excluded from the fit shown in Fig. 4.

As seen from Fig. 4, the fit underestimates the flux from Capella in the regions labeled A, B, D, and E; it overestimates the flux at the location of peak C. The latter appears to be an issue associated with location of the Fe XIX line. It was given by Brown et al. (2002) as 15.198 ± 0.005 Å, and the fit by Gu et al. (2006); Gu (2009) places it at the lower range of the experimental uncertainties, i.e. at 15.193 Å. Placing the line at the high range, i.e. at 15.203 Å, would give a much better fit.

The inclusion of the Fe XVI lines improves the fit of the Capella spectrum at the location of features B and D. Feature D is the result of a collisionally excited Fe XVI line, as discussed earlier by Beiersdorfer et al. (2012). Feature B is the result of a single Fe XVI lines, the transition $1s^2s^22p_{1/2}2p_{3/2}^4 3s_{1/2}3d_{5/2}(J = 3/2) \rightarrow 1s^2s^22p_{1/2}^2 2p_{3/2}^4 3s_{1/2}(J = 1/2)$ at 15.110 Å. This line is formed an almost equal mixture of collisional and dielectronic excitation. It also is weakly blended with an Fe XIX lines, which Brown et al. (2002) place at 15.079 ± 4 Å. This line is the closest to a pure dielectronic satellite line in the Fe XVII L-shell spectrum.

The $n = 3$ dielectronic satellite lines also add flux to other features in the spectrum. However, they do not add enough flux to fit the features labeled A and E in Fig. 4. Feature A was shown by Beiersdorfer et al. (2011) to be mainly formed by $n = 4$ dielectronic satellite lines that converge onto the $3C$ line of Fe XVII. By extension, feature E is likely formed by $n = 4$ dielectronic satellite lines that converge onto the $3D$ line of Fe XVII.

4. Conclusion

We have calculated accurate positions of the $n, n' = 3$ dielectronic satellite lines of the Fe XVII L-shell X-ray spectrum. These positions differ from current values by amounts that are several times the spectral widths of the lines recorded by *Chandra's* high energy transmission grating.

We have identified one feature, situated at 15.110 Å, that has potential for diagnostic use. A large fraction of its flux is shown to be due to the dielectronic recombination mechanism. The fraction that is due from collisional excitation can be estimated from the strength of the strongest collisionally excited Fe XVI lines, which is situated at a calculated value of 15.211 Å (Beiersdorfer et al. 2012), or at a measured values of 15.210 ± 0.04 Å (Graf et al. 2009)). This line is essentially not affected by dielectronic recombination and, thus, can be used to

detemine the abundance of sodiumlike iron. It is encouraging that the F_2 satellite strength of the line at 15.110 Å generated by our FAC calculation is the same as that produced by Nilsen (1989), as illustrated in Fig. 1. This indicates that the atomic data for this satellite line is probably reliable, although no laboratory measurements currently exist that test the accuracy of the line strength calculations for any L-shell dielectronic satellite feature. However, because the $n, n' = 3$ dielectronic line at 15.110 Å is weaker than the clusters of $n' = 4$ dielectronic satellite lines (cf. features A and E in Fig. 4), it may be preferable to use those instead for diagnostic use.

Finally, we note that the spectral fit of the Capella spectrum was improved by the inclusion of the Fe XVI collisional and dielectronic satellite lines. The temperature of Capella's corona is rather high relative to the formation temperature of sodiumlike and even of neonlike iron. The strength of the Fe XVI emission relative to that of Fe XVII is likely to be enhanced in stars with cooler coronae, such as Procyon or the Sun. Including the Fe XVI emission in the spectral fits of the X-ray emission of these stars will be, thus, even more impartant than it was for fitting the details of the Capella spectrum.

Acknowledgments

Work by the Lawrence Livermore National Laboratory was performed under the auspices of the Department of Energy under Contract No. DE-AC52-07NA-27344 and supported by NASA Astronomy and Physics Research and Analysis contract NNX12AH84G.

REFERENCES

Beiersdorfer, P. 1988, Ph.D. thesis, Princeton University

Beiersdorfer, P., Díaz, F., & Ishikawa, Y. 2012, Astrophys. J., 745, 167

Beiersdorfer, P., Gu, M. F., Lepson, J., & Desai, P. 2011, in Astronomical Society of the Pacific Conference Series, Vol. 448, 16th Cambridge Workshop on Cool Stars, Stellar Systems, and the Sun, ed. C. Johns-Krull, M. K. Browning, & A. A. West (San Francisco: Astronomical Society of the Pacific), 787

Behar, E., Cottam, J., & Kahn, S. M. 2001, Astrophys. J., 548, 966

Bitter, M., Hill, K. W., Sauthoff, N. R., Efthimion, P. C., Merservey, E., Roney, W., von Goeler, S., Horton, R., Goldman, M., & Stodiek, W. 1979, Phys. Rev. Lett., 43, 129

Bitter, M., Gu, M. F., Vainshtein, L. A., Beiersdorfer, P., Bertschinger, G., Marchuk, O., Bell, R., LeBlanc, B., Hill, K. W., Johnson, D., & Roquemore, L. 2003, Phys. Rev. Lett., 91, 265001

Brown, G. V., Beiersdorfer, P., Liedahl, D. A., Widmann, K., Kahn, S. M., & Clothiaux, E. J. 2002, Ap. J. Suppl., 140, 589

Clementson, J. & Beiersdorfer, P. 2013, Astrophys. J., 763, 54

Díaz, F., Vilkas, M. J., Ishikawa, Y., & Beiersdorfer, P. 2013, Astrophys. J., 207

Dubau, J. & Volonté, S. 1980, Rep. Prog. Phys., 43, 199

Faucher, P., Loulergue, M., Steenman-Clark, L., & Volonté, S. 1983, Astron. Astrophys., 118, 147

Foster, A. R., Ji, L., Yamaguchi, H., Smith, R. K., & Brickhouse, N. S. 2013, in American Institute of Physics Conference Series, Vol. 1545, American Institute of Physics Conference Series, ed. J. D. Gillaspy, W. L. Wiese, & Y. A. Podpaly, 252–259

Gabriel, A. H. 1972, Mon. Not. R. Astron. Soc., 160, 99

Gabriel, A. H. & Jordan, C. 1969, Nature, 221, 947

Gabriel, A. H. & Paget, T. M. 1972, J. Phys. B, 5, 673

Graf, A., Beiersdorfer, P., Brown, G. V., & Gu, M. F. 2009, Astrophys. J., 695, 818

Gu, M. F. 2008, Can. J. Phys., 86, 675

—. 2009, ArXiv e-prints, 0905.0519

Gu, M. F., Beiersdorfer, P., Brown, G. V., Graf, A., Kelley, R. L., Kilbourne, C. A., Porter, F. S., & Kahn, S. M. 2012, Canadian Journal of Physics, 90, 351

Gu, M. F., Gupta, R., Peterson, J. R., Sako, M., & Kahn, S. M. 2006, Astrophys. J., 649, 979

Ishikawa, Y. & Vilkas, M. J. 2001, Phys. Rev. A, 63, 042506

Ishikawa, Y., Quiney, H. M., & Malli, G. L. 1991, Phys. Rev. A, 63, 3270

Nilsen, J. 1989, Atomic Data and Nuclear Data Tables, 41, 131

Wargelin, B. J., Kahn, S. M., & Beiersdorfer, P. 2001, Phys. Rev. A, 63, 022710

This preprint was prepared with the AAS LaTeX macros v5.0.

Table 1. Comparison of Atomic Data for Fe XVI Lines Formed by Dielectronic Recombination.

λ^a (Å)	Transition[a]	λ_I^b (Å)	Transition[b]	$\Delta\lambda$ (Å)	F_2 (s^{-1})
15.069	21401010(1/2)→22401000(1/2)	15.068	21400101(1/2)→22401000(1/2)	.001	1.21[13]
15.090	21400020(1/2)→22400010(3/2)	15.084	21400020(1/2)→22400010(3/2)	.006	1.14[13]
15.116	21410010(3/2)→22410000(1/2)	15.110	21410001(3/2)→22410000(1/2)	.006	3.25[13]
15.158	21400101(3/2)→22400100(3/2)	15.159	21400101(3/2)→22400100(3/2)	-.001	1.85[13]
15.184	21400020(3/2)→22400010(3/2)	15.176	21400011(3/2)→22400100(3/2)	.008	2.70[13]
15.191	21400020(3/2)→22400001(5/2)	15.183	21400011(3/2)→22400001(5/2)	.008	3.23[13]
15.196	21400110(1/2)→22400100(3/2)	15.194	21400110(1/2)→22400100(3/2)	.002	1.82[13]
15.228	12420000(1/2)→22400100(3/2)	15.236	12420000(1/2)→22400100(3/2)	-.008	1.10[13]
15.233	21400011(5/2)→22400001(5/2)	15.224	21400011(5/2)→22400001(5/2)	.009	3.00[13]
15.251	21400011(7/2)→22400001(5/2)	15.231	21400011(7/2)→22400001(5/2)	.020	1.03[14]
15.258	21400002(1/2)→22400010(3/2)	15.241	21400002(1/2)→22400010(3/2)	.017	1.38[13]
15.261	22301001(3/2)→22401000(1/2)	15.257	21401010(3/2)→22401000(1/2)	.004	6.90[13]
15.280	21410001(3/2)→22410000(1/2)	15.266	21410001(3/2)→22410000(1/2)	.014	4.83[13]
15.302	21400101(5/2)→22400100(3/2)	15.290	22300101(5/2)→22400100(3/2)	.012	4.99[13]
15.316	22300101(3/2)→22401000(1/2)	15.299	21401010(3/2)→22401000(1/2)	.017	1.47[13]
15.370	21400020(5/2)→22400010(3/2)	15.345	21400020(5/2)→22400010(3/2)	.025	6.93[13]
15.397	21400002(7/2)→22400001(5/2)	15.366	21400002(7/2)→22400001(5/2)	.031	2.28[13]
15.413	21401001(5/2)→22400100(3/2)	15.414	21401001(5/2)→22400100(3/2)	-.001	7.39[12]
15.516	22300002(7/2)→22400001(5/2)	15.487	22300002(7/2)→22400001(5/2)	.029	1.95[13]
15.519	22310001(1/2)→22410000(1/2)	15.487	22310001(1/2)→22410000(1/2)	.032	7.67[12]
15.539	22300011(5/2)→22400010(3/2)	15.503	22300011(5/2)→22400010(3/2)	.036	1.54[13]

NOTES.—Occupation numbers for the $2s_{1/2}2p_{1/2}2p_{3/2}3s_{1/2}3p_{1/2}3p_{3/2}3d_{3/2}3d_{5/2}$ subshells are given to denote the upper and lower level of a given transition. The $1s_{1/2}$ shell is asummed filled in all cases. For example, 21400002 denotes the configuration $1s^2 2s^2 2p_{1/2} 2p_{3/2}^4 3d_{5/2}^2$. The total angular momentum value is given in parenthesis.

[a] Values from Nilsen (1989)

[b] Present calculation.

Fig. 1.— Comparison of the predicted strengths and positions of Fe XVI lines formed by dielectronic recombination. The calculations assume an electron density of 10^{10} cm^{-3}. Emissivities based on the atomic data from Nilsen (1989) is shown in red; those based on our calculations using FAC are shown in black.

ch

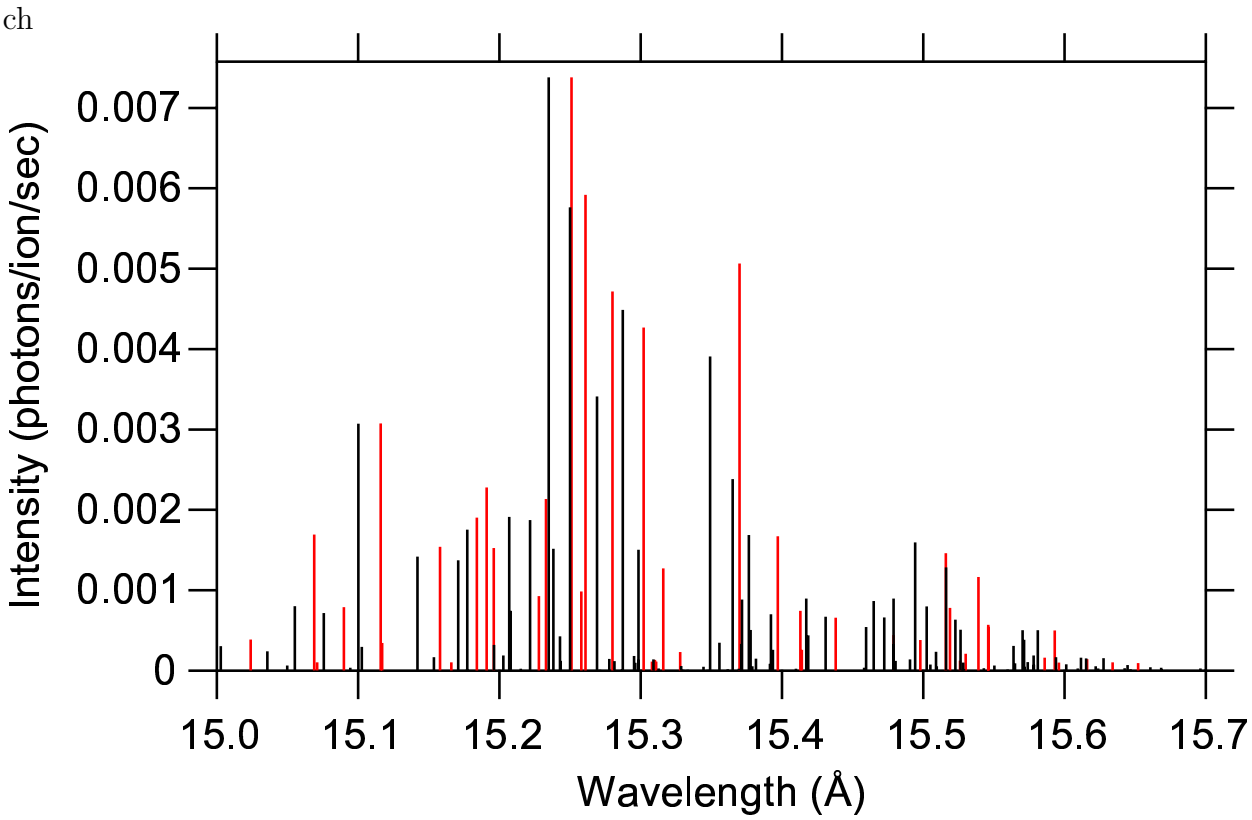

Fig. 2.— Predicted contributions to the emissivities of Fe XVI lines from collisional excitation (red line) and dielectronic recombination (green line). Black lines represent the emissivities from collisional excitation without taking into account losses due to autoionization. The calculations assume a density of 10^{12} cm^{-3}, a temperature of 600 eV, and an equal fraction of neonlike and sodiumlike iron ions.

ch

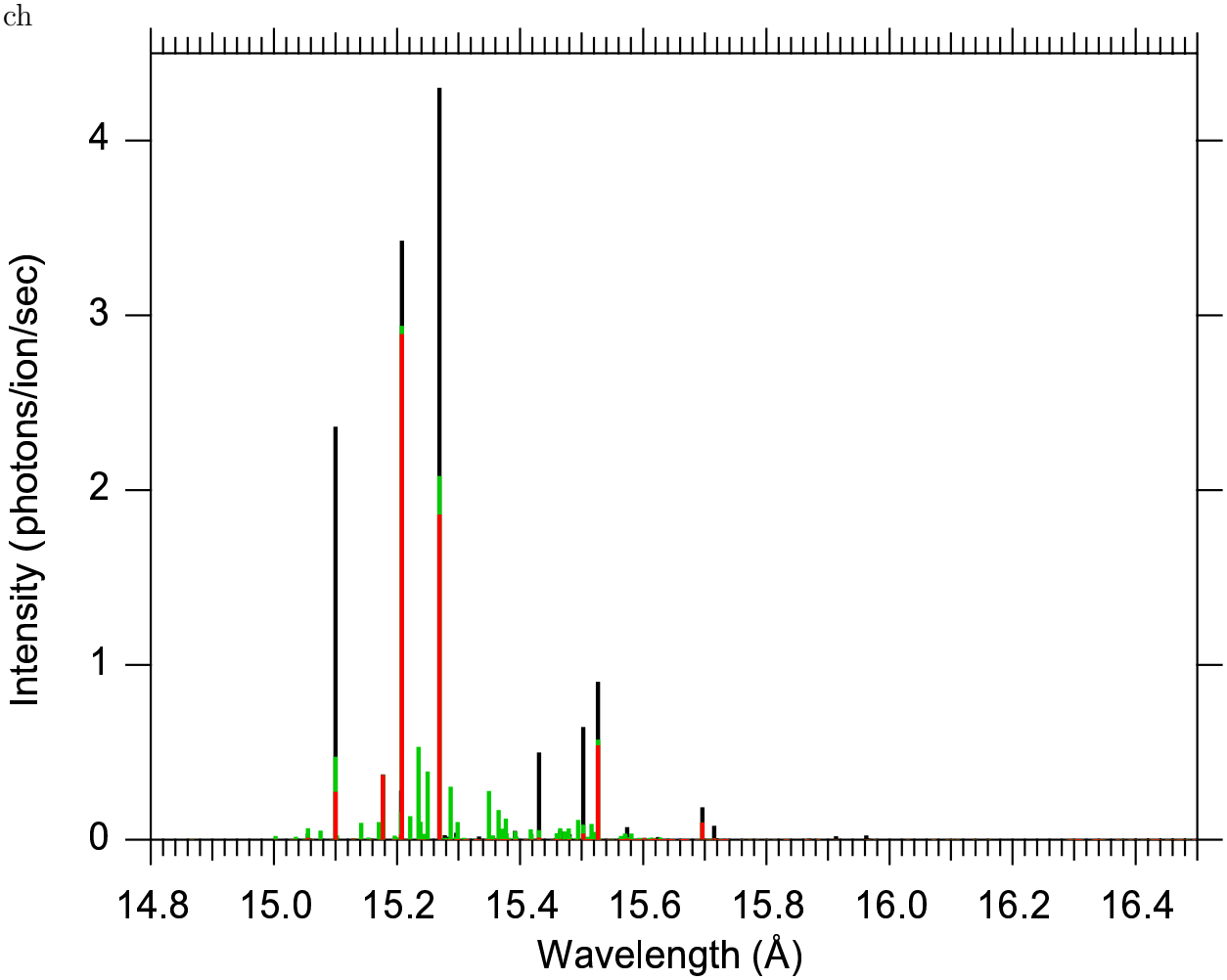

Fig. 3.— Predicted contributions to the emissivities of Fe XVI lines from collisional excitation (red line) and dielectronic recombination (green line). Black lines represent the emissivities from collisional excitation without taking into account losses due to autoionization. The calculations assume a density of 10^{12} cm^{-3}, a temperature of 600 eV, and an equal fraction of neonlike and sodiumlike iron ions.

ch

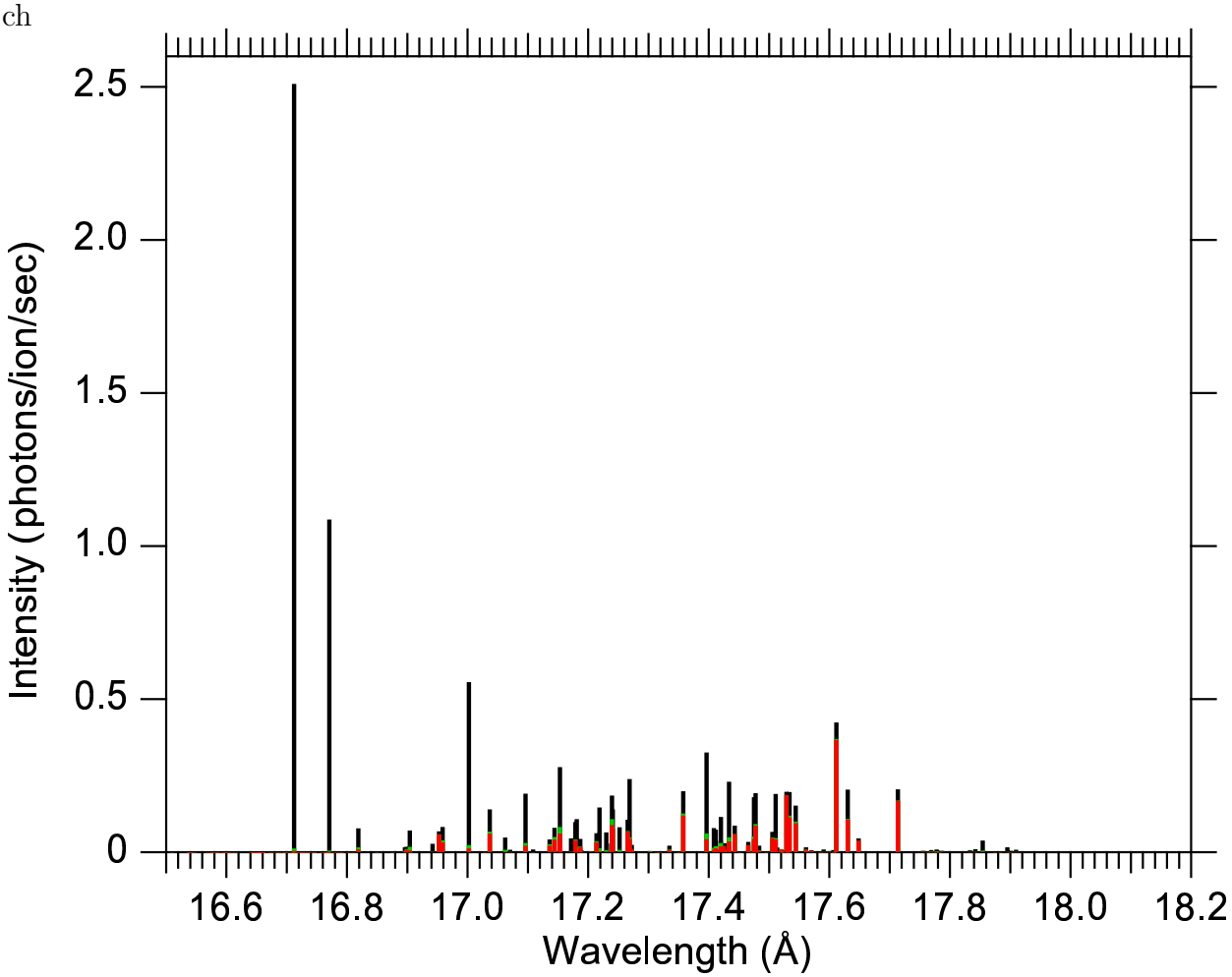

Fig. 4.— Spectrum of Capella in the region 14.9 – 15.5 Å— produced by co-adding 298 ksec of observations collected with *Chandra's* high energy transmission grating in plus and minus order (blue trace). Also shown is a fit of the spectrum (black trace) based on known spectral lines using data from ATOMDB, but excluding Fe XVI lines formed by dielectronic recombination. Inclusion of the Fe XVI collisional lines and the $n = 3$ dielectronic satellite lines produces the fit shown as a red trace. The positions of the Fe XVI, as calculated by the MRMP method, are indicated in yellow for collisionally excited lines and in green for lines formed by dielectronic recombination. Features labeled *A*–*E* are discussed in the text.

ch